THE JOURNAL OF PHYSICAL CHEMISTRY B

ARTICLE

pubs.acs.org/JPCB

A Mixed Quantum-Classical Molecular Dynamics Study of the Hydroxyl Stretch in Methanol/Carbon Tetrachloride Mixtures: Equilibrium Hydrogen-Bond Structure and Dynamics at the Ground State and the Infrared Absorption Spectrum

Kijeong Kwac and Eitan Geva*

Department of Chemistry, University of Michigan, Ann Arbor, Michigan 48109-1055, United States

ABSTRACT: We present a mixed quantum-classical molecular dynamics study of the structure and dynamics of the hydroxyl stretch in methanol/carbon tetrachloride mixtures. One of the methanol molecules is tagged, and its hydroxyl stretch is treated quantum-mechanically, while the remaining degrees of freedom are treated classically. The adiabatic Hamiltonian of the quantum-mechanical hydroxyl is diagonalized on-the-fly to obtain the corresponding adiabatic energy levels and wave functions which depend parametrically on the instantaneous configuration of the classical degrees of freedom. The dynamics of the classical degrees of freedom are in turn affected by the quantum-mechanical state of the tagged hydroxyl stretch via the corresponding Hellmann−Feynman forces. The ability of five different force-field combinations to reproduce the experimental absorption infrared spectrum of the hydroxyl stretch is examined for different isotopomers and on a wide range of compositions. It is found that, in addition to accounting for the anharmonic nature of the hydroxyl stretch, one also has to employ polarizable force fields and account for the damping of the polarizability at short distances. The equilibrium ground-state hydrogen-bonding structure and dynamics is analyzed, and its signature on the absorption infrared spectrum of the hydroxyl stretch is investigated in detail. Five different hydroxyl stretch subpopulations are identified and spectrally assigned: monomers (α), hydrogen-bond acceptors (β), hydrogen-bond donors (γ), simultaneous hydrogen-bond donors and acceptors (δ), and simultaneous hydrogen-bond donors and double-acceptors (ε). The fundamental transition frequencies of the α and β subpopulations are found to be narrowly distributed and to overlap, thereby giving rise to a single narrow band whose intensity is significantly diminished by rotational relaxation. The fundamental transition frequency distributions of the γ, δ, and ε subpopulations are found to be broader and to partially overlap, thereby giving rise to a single broad band which is red-shifted relative to the $\alpha\beta$ band. The $\gamma\delta\varepsilon$ band is also found to be inhomogeneously broadened and unaffected by rotational relaxation. The exchange rates between the different subpopulations and corresponding branching ratios are reported and explained. Finally, nonlinear mapping relations between the hydroxyl transition frequency and bond length and the electric field along the hydroxyl bond axis are established, which can be used to reduce the computational cost of the mixed quantum-classical treatment to that of a purely classical molecular dynamics simulation.

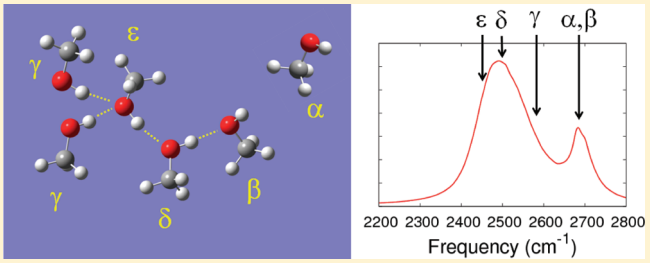

1. INTRODUCTION

Alcohols are the simplest representatives of amphiphilic compounds, which consist of a hydroxyl group capable of forming hydrogen bonds (H bonds) and an apolar alkyl tail. Thus, similar to water, alcohols form highly structured H-bonded liquids at ambient temperatures. However, alcohols typically form less H bonds per molecule in comparison to water and, unlike water, are highly miscible in apolar liquids over an extremely wide range of concentrations that extends all the way from highly dilute solutions to the bulk. Thus, mixtures of alcohols with apolar compounds form an important class of nonaqueous mixtures in which H bonding plays an important role. In fact the solubility over a wide range of concentrations in many apolar liquids, which makes it easier to control the extent of hydrogen bonding, and the smaller number of H bonds per molecule turn these mixtures into very attractive model systems for studying H bonding.

Equilibrium molecular dynamics (MD) simulations of neat alcohols and of alcohols dissolved in apolar liquids have confirmed the existence of H-bonded oligomers.[1−6] There is a very large number of possible oligomers that vary in size (i.e., number of monomers) and structure (open vs closed chain, branched vs unbranched, etc). Upon dilution in an apolar solvent, alcohols adopt an increasingly less diverse oligomer population that favors smaller linear oligomers, until the monomers become the dominant species at sufficiently high dilutions. The fact that H

Received: May 6, 2011
Revised: June 14, 2011
Published: June 16, 2011

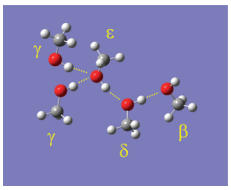

Figure 1. A cluster of hydrogen bonded methanol molecules. Each molecule is classified as α, β, γ, δ, and ε according to its H-bonding configuration, where α species represents a monomer without any H bond.

bonds break and form on the picosecond time scale implies that the above-mentioned oligomers keep fragmenting and recombining thereby giving rise to complex dynamical behavior which is still not completely understood, despite numerous experimental and theoretical studies.[5−27]

The transition frequency of the hydroxyl stretch in alcohol oligomers (3000−3800 cm^{-1} for the O−H stretch and 2300−2800 cm^{-1} for the O−D stretch) is known to be very sensitive to H bonding. As a result, the infrared (IR) spectroscopy of the hydroxyl stretch has emerged as a powerful probe of H bonding in these systems.[7,8,15−21] Figure 1 represents classification of H-bond species within an oligomer. The absorption spectrum of the hydroxyl stretch fundamental transition is known to consist of a relatively narrow high frequency feature and a broad feature which is red-shifted relative to it. The narrow feature is assigned to contributions from the monomers (α) and from hydroxyls at the end of the oligomers that serve as H bond acceptors (β). The broad and red-shifted feature is assigned to hydroxyls that serve as either H-bond donors (γ), simultaneous acceptors and donors (δ), or simultaneous double-acceptors and donors (ε). Thus, the spectral features associated with the different hydroxyl subpopulations red shift and broaden with increasing participation of the hydroxyl in H bonding. The relatively rapid rate of H bond breaking and forming implies that the transition frequencies of individual hydroxyls fluctuate both between and within those bands on a picosecond time scale.[17−21,28]

The structure and dynamics of H-bonded methanol oligomers have been the subject of several previous computational studies.[5,6,12,29−32] Ab initio calculations of isolated methanol clusters are reported in the literature.[12,29−31] In the most recent and arguably most definitive of those studies, the authors performed geometry optimizations of methanol clusters consisting of 1−7 monomers (inducing linear, cyclic, and branched structures).[31] They were then able to successfully assign the various bands in the experimental infrared (IR) spectrum of the hydroxyl stretch in dilute methanol/CCl_4 mixtures to their individual contributions from these clusters.

An alternative computational approach to studying H-bonded methanol oligomers has been based on classical MD simulations of methanol/CCl_4 mixtures.[5,6,11,32] Equilibrium structural properties and H-bond lifetimes were reported in ref 11 based on a fully classical MD simulation of methanol/CCl_4 mixtures. In this case, both methanol and CCl_4 were modeled as rigid molecules, using the nonpolarizable three-site OPLS force field for methanol[33] and a rigid five-site model for CCl_4.[34] Using a geometrical criterion for defining H bonding between methanol molecules,[3] the authors calculated the distributions of oligomers based on the number of monomers and their structure (cyclic vs linear), the average number of H bonds per methanol molecule, and the equilibrium H-bond lifetimes, as a function of methanol concentration.

Mixed quantum-classical MD simulations of methanol oligomers in a liquid of rigid CCl_4 molecules were reported in the literature.[5,6,32] In those studies, the methanol was modeled with a flexible hydroxyl stretch, described by a Morse potential. The hydroxyl stretches (one per methanol molecule) were treated quantum-mechanically, while the remaining degrees of freedom (DOF) were treated classically using nonpolarizable force fields. The Hamiltonian of the hydroxyls was diagonalized on-the-fly at each instantaneous configuration of the classical DOF, thereby yielding the instantaneous adiabatic vibrational energy levels and wave functions at each time step. Calculations were performed for the monomers, dimers, trimers, tetramers, and pentamers, including the corresponding absorption IR spectra and the rate constant for vibrational population relaxation which was described in terms of a nonadiabatic transition whose rate is given by Fermi's golden rule. The amplitude of the hydroxyl frequency fluctuations was observed to increase with increasing participation in H bonding, thereby confirming the sensitivity of the H bond to the environment (which is not accounted for in the above-mentioned ab initio studies of isolated methanol clusters). Accordingly, the bands assigned to the different subpopulations of the hydroxyl stretch in the IR absorption spectra were observed to red-shift and broaden with increasing participation in H bonding. However, in that paper, the absorption IR spectra were calculated within the framework of the Condon and second-order cumulant approximations,[35] whose validity in H-bonded systems is questionable.[36,37]

In this paper we present a mixed quantum-classical MD study of the structure and dynamics of the hydroxyl stretch in methanol/CCl_4 mixtures. Unlike the previous mixed quantum-classical treatments, we do not restrict ourselves to a single oligomer with a predetermined number of monomers and connectivity. To this end, we restrict the quantum-mechanical treatment to the photoactive hydroxyl stretch, which we refer to as the *tagged* hydroxyl, while the remaining DOF, including the other hydroxyls, are treated classically. This simplification allows us to reduce the computational cost while still being able to account for the quantum-mechanical nature of the tagged hydroxyl stretch and how it is affected by coupling with the other hydroxyls as well as the remaining DOF. We also perform a systematic comparison between force-field combinations, including polarizable ones, in order to determine which can reproduce the experimental IR absorption spectrum of the hydroxyl for different isotopomers and on a wide range of compositions. Finally, we show that it is possible to establish *nonlinear* mapping relations between the hydroxyl transition frequency and bond length and the electric field along the hydroxyl bond axis, which can be used to reduce the computational cost of the mixed quantum-classical treatment to that of a purely classical MD simulation.

The remainder of the paper is organized as follows. In section 2, we outline the mixed quantum-classical MD approach and describe the force-field combinations under consideration, simulation techniques, and the methodology used for calculating the absorption spectrum. In section 3, we present the results obtained regarding H-bonding structure and dynamics as well as its signature on the absorption IR spectrum. In section 4, we establish the nonlinear mapping relations between the transition frequency and bond length and the electric field along the hydroxyl bond axis and demonstrate how it can be used to

reproduce the absorption spectrum. Finally, the main results are summarized and the outlook is provided in section 5.

2. THEORY AND SIMULATION TECHNIQUES

A. Mixed Quantum-Classical Molecular Dynamics. Consider a methanol/CCl_4 mixture where one of the hydroxyls, referred to as the *tagged* hydroxyl, is treated *quantum-mechanically* while the remaining untagged DOF, referred to as the *bath*, are treated *classically*. The mixed quantum-classical Hamiltonian is then given by:

$$\hat{H}(\hat{q},\hat{p},\mathbf{Q},\mathbf{P}) = K_B(\mathbf{P}) + \hat{K}_q(\hat{p}) + \hat{V}(\mathbf{Q},\hat{q}) \quad (1)$$

where vectors are written in boldfaced font (e.g., $\mathbf{Q}$, $\mathbf{P}$), operators are capped (e.g., $\hat{q}$, $\hat{p}$), $\mathbf{Q}$ and $\mathbf{P}$ are the *classical* DOF coordinates and momenta, respectively, $\hat{p}$ and $\hat{q}$ are quantum-mechanical coordinate and momentum operators associated with the tagged hydroxyl stretch, respectively, $K_B(\mathbf{P})$ and $\hat{K}_q(\hat{p})$ are the bath and tagged hydroxyl stretch kinetic energies, respectively, and $\hat{V}(\mathbf{Q},\hat{q})$ is the overall potential energy.

For a given configuration of the bath DOF, $\mathbf{Q}$, we define the vibrational energy levels and corresponding stationary wave functions of the hydroxyl stretch as the eigenvalues and eigenfunctions of the *adiabatic* Hamiltonian, respectively:

$$\hat{H}_{ad}(\hat{q},\hat{p};\mathbf{Q})\Psi_n(q,\mathbf{Q}) = E_n(\mathbf{Q})\Psi_n(q,\mathbf{Q}) \quad (2)$$

where

$$\hat{H}_{ad}(\hat{q},\hat{p};\mathbf{Q}) = \hat{K}_q(\hat{p}) + \hat{V}(\mathbf{Q},\hat{q}) \quad (3)$$

and $n = 0, 1, 2,...$ correspond to the ground, first excited, second excited, etc., vibrational states of the tagged hydroxyl stretch.

In practice, the *overall* instantaneous configuration of the liquid solution is given in terms of the collection of the Cartesian coordinates of all the atoms in the simulation cell, *including the H/D atom associated with the tagged hydroxyl stretch*:

$$\begin{aligned}\mathbf{R} &= \{\mathbf{X},\mathbf{Y},\mathbf{Z}\} \equiv \{\mathbf{R}_k\} \\ &\equiv \{X_0,Y_0,Z_0,X_1,Y_1,Z_1,X_2,Y_2,Z_2,...,X_N,Y_N,Z_N\}\end{aligned} \quad (4)$$

Here $\mathbf{R}_0 = (X_0, Y_0, Z_0)$ denote the coordinates of the tagged H/D atom associated with the tagged hydroxyl and $\{\mathbf{R}_k = (X_k, Y_k, Z_k)\}$ $(k = 1, ..., N)$ are the coordinates of all the remaining atoms, including the other, H/D atoms associated with the untagged hydroxyl stretches. The corresponding atomic momenta are given by:

$$\mathbf{P} \equiv \mathbf{M}\cdot\dot{\mathbf{R}} \equiv \{M_k\dot{\mathbf{R}}_k\} \quad (5)$$

where $\mathbf{M} \equiv (M_0, ..., M_N)$ are the atomic masses. The total potential energy can then be written as

$$\begin{aligned}V(\mathbf{R}) &= V_1(X_0,Y_0,Z_0,...,X_N,Y_N,Z_N) \\ &\quad + U(X_1,Y_1,Z_1,...,X_N,Y_N,Z_N)\end{aligned} \quad (6)$$

where V_1 represents the interaction between the tagged H/D atom and the remaining atoms, and U represents all the interactions between the untagged atoms.

Within the mixed quantum-classical treatment, the Hellman−Feynman force on each of the atoms in the simulation box is explicitly dependent on the quantum state of the tagged hydroxyl stretch. Thus, when the tagged hydroxyl stretch is in the nth quantum state, the force on the kth bath atom is given by:

$$\mathbf{F}_k = -\nabla_k U - \int dq|\Psi_n(q)|^2\nabla_k V_1 \quad (7)$$

where $\nabla_k = (\partial/\partial X_k, \partial/\partial Y_k, \partial/\partial Z_k)$ and $k = 0, ..., N$. We also assume that the center of mass of the overall system is stationary so that the total force vanishes:

$$\sum_{k=0}^{N}\mathbf{F}_k = 0. \quad (8)$$

Importantly, for a given *overall* configuration, $\mathbf{R}$, the value of q is uniquely determined, whereas knowledge of the adiabatic Hamiltonian, $\hat{H}_{ad}(\hat{q},\hat{p};\mathbf{Q})$, requires knowledge of the explicit dependence of the potential energy on q for a given $\mathbf{Q}$ (see eq 3). Thus, in order to obtain the latter from the former, we evaluate the potential energy along a 41 point 1D grid of q values in the range 0.46 Å $\le q \le$ 1.46 Å by modifying $\mathbf{R}_0$ in such a way that only q changes while the remaining coordinates, including the C−O−H/C−O−D bending angle and the dihedral angles associated with the tagged hydroxyl, are constrained at their original values. It should also be noted that after $\hat{H}_{ad}(\hat{q},\hat{p};\mathbf{Q})$ is diagonalized, the values of $\mathbf{R}_0$ can be reset so as to be consistent with the expectation value of $\hat{q}$ with respect to the new stationary state, $\overline{q}=\langle\Psi_n|\hat{q}|\Psi_n\rangle$. To this end, we employ the SHAKE algorithm in order to constrain the value of q at its expectation value $\overline{q}$. It should be noted that in this case, the SHAKE algorithm is *not* used in order to constrain the bond length to a preassigned constant value. Instead, the SHAKE algorithm is used in order to *adjust* the bond length to the value $\overline{q}$ which varies from one time step to another.

The above considerations lead to the following mixed quantum-classical MD algorithm:

1. Start the ith step with a given set of initial atomic coordinates, $\mathbf{R}^{(i)}$, and momenta, $\mathbf{P}^{(i-1/2)}$, as obtained at the end of the previous step.
2. Generate the adiabatic Hamiltonian, $\hat{H}_{ad}'$, that correspond to $\mathbf{R}^{(i)}$.
3. Solve eq 2 with $\hat{H}_{ad}'$ for $\{\Psi_n'\}$ and $\{E_n'\}$.
4. Use $\{\Psi_n'\}$ in order to calculate the Hellmann−Feynman forces, $\{\mathbf{F}_k^{(i)}\}$, eq 7.
5. Update the velocities and coordinates according to:

$$\begin{aligned}\mathbf{P}'^{(i+1/2)} &= \mathbf{P}^{(i-1/2)} + \Delta t\mathbf{F}^{(i)} \\ \mathbf{R}'^{(i+1)} &= \mathbf{R}^{(i)} + \Delta t M^{-1}\cdot\mathbf{P}'^{(i+1/2)}\end{aligned} \quad (9)$$

   where Δt is the time step and $\mathbf{M}^{-1} = (M_0^{-1}, ..., M_N^{-1})$.
6. Apply the SHAKE method in order to constrain the value of q to $\overline{q}' = \langle\Psi_n'|\hat{q}|\Psi_n'\rangle$ and to constrain any rigid bonds in bath DOF, thereby readjusting the coordinates from $\mathbf{R}'^{(i+1)}$ into $\mathbf{R}''^{(i+1)}$.
7. Generate the adiabatic Hamiltonian, H_q'', that correspond to $\mathbf{R}''^{(i+1)}$.
8. Solve eq 2 with H_q'' for $\{\Psi_n''\}$ and $\{\tilde{E}_n''\}$.
9. Calculate the new expectation value of $\hat{q}$, $\overline{q}'' = \langle\Psi_n''|\hat{q}|\Psi''_n\rangle$.
10. Apply the SHAKE method in order to readjust q to $\overline{q}''$, which corresponds to adjusting the coordinates from $\mathbf{R}''^{(i+1)}$ into $\mathbf{R}^{(i+1)}$.

dx.doi.org/10.1021/jp204245z |J. Phys. Chem. B 2011, 115, 9184–9194

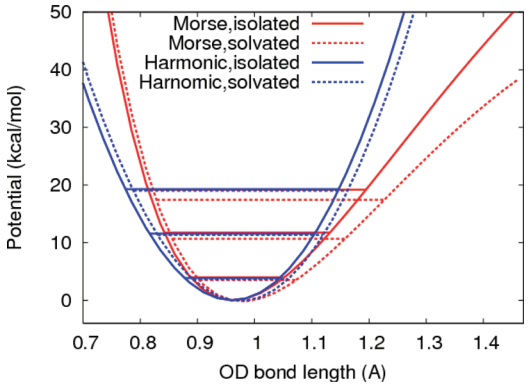

Figure 2. Potential energy curves for the OD stretch. Shown are the anharmonic Morse potential for the hydroxyl stretch employed in this work alongside the standard AMBER harmonic potential. Both potentials are shown for the isolated as well as for the solvated stretch (the latter in the case of a 10 mol % CH_3OD/CCl_4 mixture, obtained by averaging over 50 000 configurations taken from a 50 ps mixed quantum-classical MD trajectory using the polarizable force fields described below). Also shown are the energy levels of the corresponding ground, first excited, and second excited states in the case of an OD stretch.

11. Update the momenta:

$$\mathbf{P}^{(i+1/2)} = \mathbf{P}'^{(i+1/2)} + \frac{\mathbf{R}^{(i+1)} - \mathbf{R}'^{(i+1)}}{\Delta t} \qquad (10)$$

12. Return to step 1 in order to start the next step.

It should be noted that the SHAKE method is applied twice within each time step. The first application in step 6 is based on the value of $\overline{q}$ which is consistent with the configuration at the previous time step. The second application in step 10 is based on the value of $\overline{q}$ which is consistent with the configuration at the current time step.

All the simulations reported in this paper were carried out using the AMBER 10 program package.[38] However, the source code of the AMBER 10 program package needed to be modified in order to implement this algorithm.

B. Force Fields. As we will show below, the anharmonicity of the tagged hydroxyl stretch must be accounted for in order to reproduce the absorption spectrum. It is therefore assumed to be governed by a Morse potential of the form:

$$V_{vib}(q) = D_0[1 - e^{-a(q-q_0)}]^2 \qquad (11)$$

where D_0 is the bond dissociation energy and q_0 is the equilibrium bond length. The bond length was set to q_0 = 0.96131 Å based on the optimized equilibrium geometry of a single methanol molecule as obtained from an electronic structure calculation using density functional theory (DFT) with the B3LYP functional and 6-311++G(p,d) basis set. The bond dissociation energy was adopted from ref 39 and set equal to D_0 = 105.0 kcal/mol. Finally, the value of the parameter a was set to a = 2.40414 $Å^{-1}$ as obtained by best fitting of the fundamental transition frequency to its experimental gas-phase value of 2717.6 cm^{-1}.[40] It should be noted that the remaining untagged hydroxyl stretches are treated as harmonic using the standard AMBER force-field parameters (i.e., spring constant of K_r = 553 kcal/(mol $Å^2$) and equilibrium length of r_{eq} = 0.96 Å).

In Figure 2, we compare the anharmonic Morse potential for the OD stretch employed in this work with the standard AMBER harmonic potential. Both potentials are shown for the isolated as well as for the solvated stretch (the latter in the case of a 10 mol % CH_3OD/CCl_4 mixture, obtained by averaging over 50 000 configurations taken from a 50 ps mixed quantum-classical MD trajectory using the polarizable force fields described below). Also shown are the energy levels of the corresponding ground, first excited, and second excited states in the case of an OD stretch. It should be noted that the anharmonic hydroxyl stretch potential is more sensitive to solvation than the harmonic potential. For example, while the fundamental harmonic transition frequency red-shifts from 2698.0 cm^{-1} in the isolated CH_3OD (denoted as MeOD from now on) to 2678.5 cm^{-1} in the solvated MeOD, i.e., a red shift of ~20 cm^{-1}, the fundamental and overtone anharmonic transition frequencies red-shifted from 2710.8 cm^{-1} and 2601.8 cm^{-1}, respectively, in the isolated MeOD to 2499.4 cm^{-1} and 2369.5 cm^{-1}, respectively, in the solvated MeOD, i.e., red shifts of ~210 cm^{-1} and ~240 cm^{-1}, respectively. These red shifts are also sensitive to whether one uses polarizable or nonpolarizabe force fields. For example, switching to nonpolarizable force fields reduces the red-shift of the fundamental frequency from ~210 cm^{-1} to ~190 cm^{-1}. Another important feature of the anharmonic hydroxyl stretch potential is that the equilibrium bond length *increases* upon solvation, and more so for the excited state than the ground state. Thus, one expects vibrational excitation to increase the propensity for forming H bonds.

The remaining contributions to the potential energy are given by:

$$V = \sum_{bonds} K_r(r - r_{eq})^2 + \sum_{angle} K_\theta(\theta - \theta_{eq})^2 + \sum_{dihedral} \frac{V_n}{2}[1 + cos(n\phi - \gamma)] + \sum_{i<j} 4\varepsilon_{ij}\left[\left(\frac{\sigma_{ij}}{R_{ij}}\right)^{12} - \left(\frac{\sigma_{ij}}{R_{ij}}\right)^{6}\right] + \sum_{i<j}\frac{q_i q_j}{\varepsilon R_{ij}} + E_{pol} \qquad (12)$$

Here, K_r, K_θ, and V_n are force constants for bonds, angles, and dihedral terms, r_{eq} and θ_{eq} are equilibrium values for bond lengths and angles; n is the dihedral multiplicity, γ is the dihedral angle phase; ε_{ij} and σ_{ij} are Lennard–Jones potential parameters for ith and jth atoms, q_i is the charge of the ith atom, and ε is the permittivity.

E_{pol} in eq 12 represents the contribution to the potential energy due to polarization and is used when polarizable force fields are used. This term is given by:[41]

$$E_{pol} = -\frac{1}{2}\sum_i m_i \cdot \mathbf{E}_i^0 \qquad (13)$$

where

$$\mu_i = \alpha_i \mathbf{E}_i \qquad (14)$$

$$\mathbf{E}_i = \mathbf{E}_i^0 + \sum_{j(\neq i)} \mathbf{T}_{ij} \cdot \mu_j \qquad (15)$$

$$\mathbf{E}_i^0 = \sum_{j(\neq i)} \frac{q_j \mathbf{r}_{ij}}{r_{ij}^3} \qquad (16)$$

$$\mathbf{T}_{ij} = \frac{1}{r_{ij}^3}\left(\frac{3\mathbf{r}_{ij} \cdot \mathbf{r}_{ij}}{r_{ij}^2} - 1\right) \qquad (17)$$

Here, α is the atomic polarizability, $\mathbf{E}_i$ is the total electric field at atom i, $\mathbf{E}_i^0$ is the electric field at atom i produced by the fixed charge in the system, and $\mathbf{T}_{ij}$ is the dipole tensor.

dx.doi.org/10.1021/jp204245z |J. Phys. Chem. B 2011, 115, 9184–9194

Table 1. Force-Field Parameters for Methanol

atom type	σ (Å)	ε (kcal/mol)	charge	α (Å^3)
H	2.4714	0.0157	0.032736	0.135
C	3.3997	0.1094	0.102608	0.878
O	3.0665	0.2104	−0.571736	0.465
D	0.0	0.0	0.370920	0.135
bonds		K (kcal/(mol Å^2)$^{-1}$)		R_{eq}(Å)
H−C		340.0		1.09
C−O		320.0		1.41
O−D		553.0		0.96
angle		K_θ (kcal/(mol radian^2))		θ_{eq} (deg)
H−C−O		50.0		109.5
C−O-D		55.0		108.5
dihedral		$V_n/2$ (kcal/mol)	γ (deg)	n
H−C−O-D		0.5/3	0.0	3.0

Table 2. Force-Field Parameters for CCl_4

atom type	σ (Å)	ε (kcal/mol)	charge	α (Å^3)
C	3.80	0.050	0.248	0.878
Cl	3.47	0.266	−0.062	1.910
bonds		K (kcal/(mol Å^2)$^{-1}$)		R_{eq}(Å)
C−Cl		245.0		1.781
angle		K_θ (kcal/(mol radian^2))		θ_{eq} (deg)
Cl−C−Cl		50.0		109.5

The force-field parameters used in this work for methanol and CCl_4 are shown in Tables 1 and 2, respectively. The parameters for the methanol are taken from the AMBER force fields[38] and those for CCl_4 were adopted from ref 42. The polarizabilities, α, in Tables 1 and 2 were adopted from ref 43. However, when polarizable force fields are used, the AMBER partial charges of methanol are multiplied by a scale factor of 0.88 as recommended by Caldwell and Kollman.[41]

C. Damping Procedure for the Polarizable Force Fields. Assigning specific *constant* values of the polarizability to each atom can result in unreasonably large induced dipole moments at sufficiently small interatomic distances. While this usually does not pose a problem in classical MD simulations,[44] this is not the case for mixed quantum-classical simulations. This is because quantum delocalization of the H/D atom allows it access to classically forbidden regions where it comes to be in close proximity with neighboring atoms. More specifically, the need to calculate the potential surface on a relatively wide range of hydroxyl stretch coordinate displacements makes the calculation of interactions at relatively short and classically forbidden interatomic distances inevitable.

Figure 3 shows the divergence at short distances of the total dipole moment of a pair of methanol molecules as a function of the intermolecular distance along the H-bond axis when the standard polarizable force fields are used. In contrast, an ab initio calculation of the same dipole moment via DFT, using the B3LYP functional and 6-311++G(p,d) basis set, reveals the physically expected behavior, where the overall dipole *decreases* at short distances ($\leq$1.0 Å).[45,46] In order to account for this effect, we adopt the procedure proposed by Thole[47] and by Levy and co-workers[45] for damping the polarizable force-field parameters at short distances. The damping corresponds to a decrease in the atomic polarizabilities at short distances due to the overlap of electronic densities. To this end, we modified the dipole−dipole interaction tensor in the following manner:[46−48]

$$\mathbf{T}_{ij} = \left(f_{ij}^{t} \frac{3\mathbf{r}_{ij}\mathbf{r}_{ij}}{r_{ij}^{5}} - \frac{f_{ij}^{e}}{r_{ij}^{3}} \right) \tag{18}$$

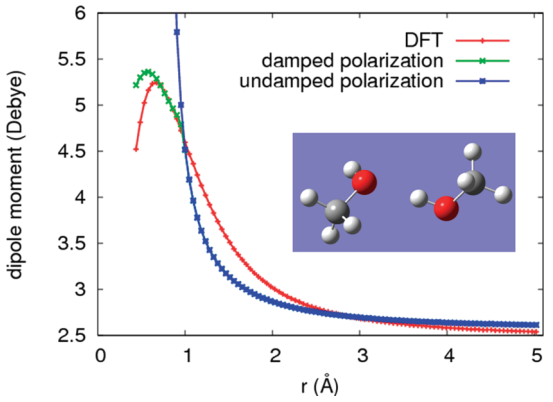

Figure 3. The total dipole moment of a pair of methanol molecules as a function of the H-bond distance. The H-bond distance was changed by translating one methanol molecule relative to another along the vector connecting the two oxygen atoms (see insert).

where f_{ij}^{e} and f_{ij}^{t} are distance-dependent screening functions adopted from ref 47 and defined as follows:[45]

$$f_{ij}^{e} = \begin{cases} 1.0 & \text{if } r_{ij} > s_{ij} \\ 4w_{ij}^{3} - 3w_{ij}^{4} & \text{if } r_{ij} < s_{ij} \end{cases}, \quad f_{ij}^{t} = \begin{cases} 1.0 & \text{if } r_{ij} > s_{ij} \\ w_{ij}^{4} & \text{if } r_{ij} < s_{ij} \end{cases} \tag{19}$$

Here,

$$w_{ij} = \frac{r_{ij}}{s_{ij}} + \frac{1}{m}\left[1 - \left(\frac{r_{ij}}{s_{ij}}\right)^{m}\right] \tag{20}$$

and

$$s_{ij} = a(\alpha_i \alpha_j)^{(1/6)} \tag{21}$$

We set $m = 32$ and $a = 1.662$ and use an expression for the electric field which takes into account the distance-dependent attenuation or shielding of charges when two atoms are close to each other:[45]

$$E_i^0 = \frac{1}{4\pi\varepsilon_0} \sum_j \left\{ 1 - exp\left[-\gamma \left(\frac{r_{ij}}{s_{ij}} \right)^{n} \right] \right\} \frac{q_j}{r_{ij}^2} \tag{22}$$

The values of the parameters in eq 22 were set to $\gamma = 5.8$ and $n = 3$ and were obtained by best fitting to to the damped total dipole moment obtained via the ab initio calculation (see Figure 3).

D. Simulation Details. Most of the results reported below were obtained from *ground state mixed quantum-classical* simulations

dx.doi.org/10.1021/jp204245z |J. Phys. Chem. B 2011, 115, 9184–9194

that were carried out at 300 K for a 10 mol% mixtures consisting of 26 MeOD molecules and 230 CCl_4 molecules in a cubic box with periodic boundary conditions whose size is adjusted by a 800 ps classical 1.0 atm constant pressure trajectory. The system was equilibrated at 300 K over 200 ps using classical MD using Langevin dynamics with the collision frequency set to 1.0 ps^{-1}. Following that, initial configurations for mixed quantum-classical MD simulations were chosen every 2 ps in order to avoid correlations. Furthermore, different randomly chosen methanol molecules were tagged in order to eliminate correlations and enhance sampling efficiency.

For each initial configuration thus obtained, a two step-equilibration procedure was followed. In the first step, we randomized the initial velocities of the system by reassigning them from a Maxwellian distribution at 300 K, followed by a 200 ps 300 K constant temperature classical MD simulation using Langevin dynamics with the collision frequency of 1.0 ps^{-1}. In the second step, a 35 ps 300 K constant temperature mixed quantum-classical trajectory was run using the weak-coupling algorithm of Berendsen et al.[49] Following equilibration, 400 50 ps mixed quantum-classical constant energy production runs were carried out, starting from 400 different initial configurations. These production runs were used to generate the absorption spectra reported below.

In the analysis of H-bond structure and dynamics, the following criteria were used to define a H bond: (1) O···D distance is less than 2.65 Å and (2) O···D−O angle is greater than 120° ("···" denotes the H-bond).

E. IR Absorption Spectrum. Within the mixed quantum-classical treatment, the IR absorption spectrum is calculated based on the following formula:[35]

$$I(\omega) = Re\int_0^\infty dt J(t) exp(i\omega t) \tag{23}$$

where, $J(t)$ is the linear optical response function (ORF) given by:[35]

$$J(t) = \langle \vec{V}_{01}(t)\cdot \vec{V}_{10}(0)\, exp[-i\int_0^t d\tau\omega_{10}(\tau)]\rangle \tag{24}$$

Here,

$$\langle\cdots\rangle = \frac{1}{Z_0}\int d\mathbf{Q}_0 \int d\mathbf{P}_0 exp[-\beta H_0(\mathbf{Q}_0,\mathbf{P}_0)]\cdots \tag{25}$$

where $H_0(\mathbf{Q}_0, \mathbf{P}_0) = K_B(\mathbf{P}_0) + E_0(\mathbf{Q}_0)$ is the bath Hamiltonian when the tagged hydroxyl stretch is at the ground state, $Z_0 = \int d\mathbf{Q}_0 \int d\mathbf{P}_0 \exp[-\beta H_0(\mathbf{Q}_0, \mathbf{P}_0)]$ is the corresponding canonical classical bath partition function, $\{\mathbf{Q}_0, \mathbf{P}_0\}$ are the initial bath positions and momenta, $\vec{V}_{10}(t)$ is the transition dipole moment vector whose magnitude is given by $\langle\Psi_1(\mathbf{Q}_t)|\hat{q}|\Psi_0(\mathbf{Q}_t)\rangle$ and which is aligned along the hydroxyl stretch, $\omega_{10}(t) = [E_1(\mathbf{Q}_t) - E_0(\mathbf{Q}_t)]/\hbar$ is the fundamental transition frequency and $\{\mathbf{Q}_t, \mathbf{P}_t\}$ are obtained via classical dynamics on the ground state potential surface, $E_0(\mathbf{Q})$, with $\{\mathbf{Q}_0, \mathbf{P}_0\}$ as the initial conditions.

It should be noted that $J(t)$ in eq 24 is sensitive to fluctuations of the transition frequency, $\omega_{10}(t)$, and dipole moment, $\vec{V}_{10}(t)$. Within the commonly used *Condon approximation*, one neglects the fluctuations of the transition dipole moment, which amounts to replacing it by its average value, $\langle\vec{V}_{01}(t)\cdot\vec{V}_{10}(0)\rangle \approx \langle|V_{10}|^2\rangle$, so that

$$J(t)\approx J^C(t) = \langle|V_{10}|^2\rangle\langle exp[-i\int_0^t d\tau\omega_{10}(\tau)]\rangle \tag{26}$$

Table 3. Force-Field Combinations

name	OD bond for quantum DOF	polarizability	damping
AA	Amber (harmonic)	no	no
AdpA	Amber (harmonic)	yes	yes
MA	Morse	no	no
MpA	Morse	yes	no
MdpA	Morse	yes	yes

Table 4. Peak Positions and fwhm of δ OD Stretch Frequency Distributions As Obtained Using Different Force Field Combinations

name	position of max. (cm^{-1})	fwhm (cm^{-1})
AA	2678.7	24.6
AdpA	2677.0	30.6
MA	2513.2	134.2
MpA	2537.3	153.8
MdpA	2505.1	175.0
experiment[20]	~2490	~150

Finally, in the limit of inhomogeneous broadening, one also neglects the fluctuations of the transition frequency, $\omega_{10}(\tau) \approx \omega_{10}(0)$, so that:

$$J(t)\approx J^{inh}(t) = \langle|V_{10}|^2\rangle\langle exp[-i\omega_{10}(0)t]\rangle \tag{27}$$

In this limit, the absorption spectrum reflects the ground-state equilibrium distribution of fundamental transition frequencies.

3. RESULTS AND DISCUSSION

We have considered the five different combinations of force fields listed in Table 3. As we will show below, the force-field combination that best captures the experimental absorption spectrum of the hydroxyl stretch in methanol/CCl_4 mixtures is the one denoted by MdpA (Morse-damped-polarizable-Amber), which combines the Morse potential for the tagged hydroxyl stretch and polarizable AMBER force fields including damping as given by eqs 18 and 22. The combination denoted MpA (Morse-polarizable-Amber) corresponds to anharmonic Morse potential and polarizable force fields without damping. The MA (Morse-Amber) combination still used the Morse potential but differs from the MpA combination by the fact that the polarizable force fields are replaced by nonpolarizable force fields. The AdpA (Amber-damped-polarizable-Amber) combination is the same as MdpA except the fact that the harmonic Amber potential is used for the tagged hydroxyl stretch. Finally, the AA (Amber−Amber) combination is obtained from the AdpA combination by turning off the polarizability and damping. For the cases of polarizable force fields, the partial charges of methanol are scaled by 0.88, but for the nonpolarizable force fields, the standard Amber partial charges are used.

A. Radial Distribution Functions. Figure 4 shows the D−D and D−O radial distribution functions (RDFs) involving the D of the tagged OD stretch and the D or O of a neighboring methanol molecule. The prominent first peaks at 1.73−1.83 Å for the O−D RDF and 2.43−2.52 Å for the D−D RDF can be traced back to H bonding. The height of the first peak for the O−D RDF ordered from highest to lowest, and thereby from maximal to minimal H bonding, is as follows: MA(3.249) > MdpA(3.089) ~ AA(3.048) > AdpA(2.537) > MpA(2.435). The height of the

dx.doi.org/10.1021/jp204245z |J. Phys. Chem. B 2011, 115, 9184–9194

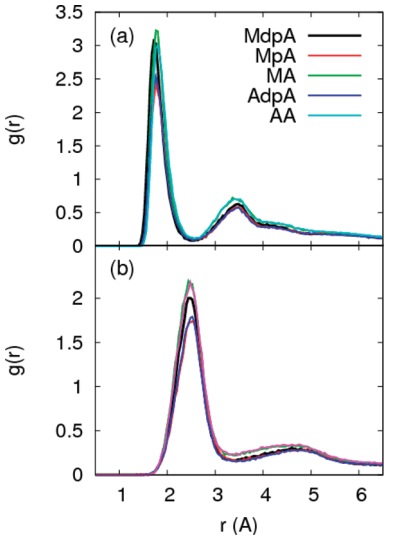

Figure 4. The D−O (a) and D−D (b) radial distribution functions involving the D of the tagged OD stretch and the D or O of a neighboring methanol molecule.

Table 5. Relative Populations (in %) of H-Bonded Species (α, *β*, *γ*, *δ*, *ε*) As Obtained Using Different Force-Field Combinations[a]

species	AA	AdpA	MA	MpA	MdpA
α	5.6	18.5	5.4	17.4	12.0
β	6.0	8.9	5.0	10.3	7.3
γ	11.9	15.2	10.9	15.0	15.7
δ	69.3	51.6	71.7	51.9	58.8
ε	6.4	5.1	6.3	4.6	5.6

[a] See Figure 1 for the configuration of H bonding of each species.

first peak for the D−D RDF ordered from highest to lowest follows a similar trend: MA(2.195) > AA(2.180) ∼ MdpA-(2.022) > AdpA(1.809) > MpA(1.793). This trend seems to suggest that the propensity for H bonding is higher in the case of the nonpolarizable force fields (MA, AA) than in the case of polarizable force fields (MdpA, MpA, AdpA). This trend can be traced back to the fact that the methanol partial charges are scaled by 0.88 in the case of the polarizable force fields thereby weakening the propensity for H bonding. It should also be noted that other than the difference in height of the first peak, the overall shapes of the RDFs and peak locations are relatively insensitive to the choice of force-field combination.

B. Hydrogen Bonding. The subpopulations of the different H-bonded species as obtained for different force-field combinations are listed in Table 5 for the case of 10 mol% MeOD/CCl_4. The largest subpopulation corresponds to the *δ* species for all force-field combinations. The *δ* subpopulation is also seen to decrease at the expense of the α and *β* subpopulations upon switching from nonpolarizable to polarizable force fields. This trend, too, can be traced back to scaling the methanol partial charges by a factor of 0.88 in the polarizable force fields, which lowers the propensity for forming H bonds. Another interesting observation is the non-negligible *ε* subpopulation of about 5.1−6.4%.

Comparing the results obtained for the AA and MA force fields, one observes that the extent of H bonding is not affected by accounting for the anharmonicity of the hydroxyl stretch (see Table 5). However, it should be noted that including the anharmonicity is indispensible for quantitatively reproducing the spectral signature of H bonding (see below).

Table 6. Branching Ratios for H-Bond Breaking and Forming Processes[a]

	to			
from	α	*β*	*γ*	*δ* + *ε*
α	0.0	37.2	62.6	0.2
β	26.0	0.0	0.0	74.0
γ	29.8	0.0	0.0	70.2
δ + *ε*	0.0	42.8	57.2	0.0

[a] The entries in the table show the probability of each product species starting from each reactant species in the left column.

As we explain below, the best agreement with the experimental absorption spectrum is obtained by using the MdpA force-field combination. For this case, we find the following average lifetimes of different H-bonded species: α: 0.77 ps, *β*: 0.33 ps, *γ*: 0.49 ps, *δ*: 0.82 ps, and *ε*: 0.18 ps. If we treat the *δ* and *ε* as a single species, the lifetime of *δ* + *ε* is 1.16 ps. As expected, the lifetime increases with increasing H-bond strength. The branching ratios of H-bonding breaking and forming events are summarized in Table 6. For the *δ* species, which are the longest lived, breaking a H bond can occur either on the donor side, in which case it will turn into a *γ* species, or on the acceptor side, in which case it will turn into a *β* species. The 57.2:42.8 branching ratio indicates that breaking the donor H-bond is somewhat more likely. A *γ* species can only break a H bond on the acceptor side, thereby turning into an α species, or form another H bond as a donor, thereby turning into a *δ* species. The branching ratio of 29.8:70.2 implies that forming a H bond is about three times more likely. A *β* species can only break a H bond as a donor, thereby turning into an α species, or form another H bond as an acceptor, thereby turning into a *δ* species. The branching ratio of 26.0:74.0 implies that here, too, forming a H bond is about three times more likely. Finally, an α species can form a H bond as either an acceptor, thereby turning into a *β* species, or as a donor, thereby turning into a *γ* species, or both, thereby turning into a *δ* species. The branching ratio of 37.2:62.6:0.2 implies that donating a H bond is about two times more likely than accepting a H bond and that the probability for forming two H bonds simultaneously, as both donor and acceptor, is negligibly small.

C. IR Absorption Spectrum. In Figure 5 we also show the distribution of the OD stretch frequencies for the case of 10 mol% MeOD/CCl_4, with a breakdown to the different H-bonded species for the case of the MdpA force-field combination. Other force-field combinations give rise to similar distributions although the positions and widths of the distributions are different. The corresponding positions of the maxima and fwhm of the *δ* OD stretch frequency distributions are listed in Table 4. From Table 4 we see that both red shift and fwhm of the *δ* OD stretch frequency distribution are significantly underestimated when one attempts to describe the tagged OD stretch by a harmonic potential. The effect of using polarizable force fields is also negligible when one uses a harmonic OD stretch potential. In contrast, describing the tagged OD stretch in terms of a Morse potential significantly increases the red shift and fwhm from ∼21−17 cm^{-1} and ∼24−30 cm^{-1} to 187 cm^{-1} and 134 cm^{-1}, respectively

dx.doi.org/10.1021/jp204245z |J. Phys. Chem. B 2011, 115, 9184–9194

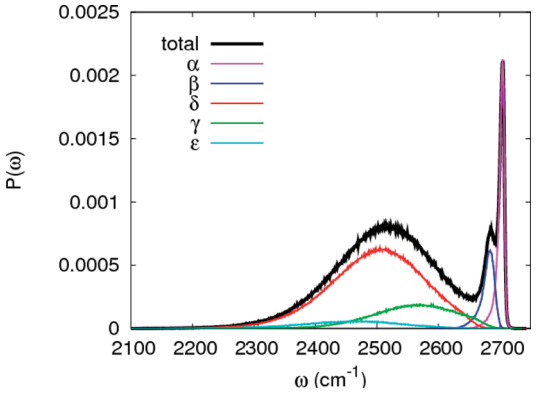

Figure 5. The probability density of the OD stretch frequencies for the case of 10 mol% MeOD/CCl_4, with a breakdown to the different H-bonded species for the case of the MdpA force-field combination.

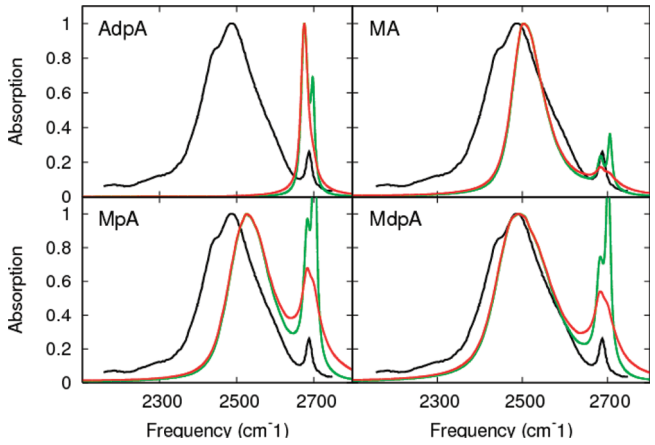

Figure 6. The IR absorption line shape of 10 mol% MeOD/CCl_4 as calculated using eqs 23 and 24 with the AdpA, MA, MpA, and MdpA force-field combinations (red). Also shown are the corresponding line shapes in the Condon approximation, eq 26 (green), and the experimental line shape (black).

(see MA in Table 4). Furthermore, in this case, switching from nonpolarizable to polarizable force fields and accounting for the damping of the polarizability at short distances further increases the red shift and fwhm to 195 cm^{-1} and 175 cm^{-1}, respectively (see MdpA in Table 4).

The IR absorption line shape of 10 mol% MeOD/CCl_4 was calculated using eqs 23 and 24 with the AdpA, MA, MpA, and MdpA force-field combinations. The results are shown and compared to the corresponding experimental spectrum[20] in Figure 6. All the spectra were normalized so that the maximal absorption is set to unity. The experimental spectrum consists of a pronounced broad peak centered at 2490 cm^{-1} and with a fwhm of 150 cm^{-1}, which was assigned to the γ, δ, and ε subpopulations, and a less pronounced narrow peak centered at 2690 cm^{-1}, which was assigned to the α and β subpopulations. It should also be noted that the shoulder at 2440 cm^{-1} was assigned to a Fermi resonance which is not accounted for in our model.

The position of the maximal absorption peak and fwhm are extremely sensitive to the choice of force-field combination and given by 2678.9 cm^{-1} and 16.9 cm^{-1} (AA), 2675.3 cm^{-1} and 23.2 cm^{-1} (AdpA), 2502.3 cm^{-1} and 88.3 cm^{-1} (MA),

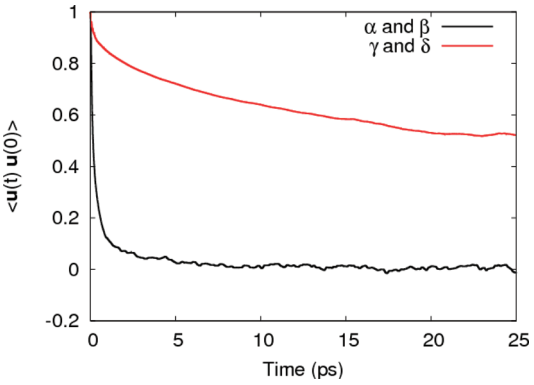

Figure 7. The time correlation functions of the unit vector along the OD bond for the $\alpha\beta$ (black) and $\gamma\delta\varepsilon$ (red) subpopulations.

2525.8 cm^{-1} and 128.0 cm^{-1} (MpA), and 2490.5 cm^{-1} and 149.0 cm^{-1} (MdpA), respectively. The trends are similar to those observed for the distributions of the OD stretch frequency, and the best, and reasonably good, agreement with experiment is obtained by using the MdpA force-field combination. This implies that describing the tagged OD stretch in terms of a Morse potential and employing polarizable force fields *with damping* are necessary to reproduce the experimental IR absorption spectrum.

Also shown in Figure 6 are the IR absorption line shapes as obtained within the Condon approximation. While the broad $\gamma\delta\varepsilon$ peak appears to be relatively insensitive to this approximation, and is in fact inhomogeneously broadened, the $\alpha\beta$ peak is observed to become significantly larger within the Condon approximation. This observation signals rapid fluctuation of the transition dipole moment in the α and β species, which can be traced back to the more rapid rotational relaxation of the monomers and small oligomers. This was verified by calculating the time correlation function of the unit vector along the OD bond for the $\alpha\beta$ and $\gamma\delta\varepsilon$ subpopulations (see Figure 7). As expected, the rotational correlation time for the $\alpha\beta$ subpopulation, ~0.48 ps, is very short and within the time scale of the relaxation of $J(t)$. In contrast, the rotational correlation time for the $\gamma\delta\varepsilon$ subpopulation is 28.84 ps and much longer than the time scale of the relaxation of $J(t)$.

Finally, it should be noted that despite the relative success of the MdpA force-field combination in reproducing the absorption spectrum without adjustable parameters, there are still a few aspects of the experimental spectrum that are not captured. In particular the MdpA force-field combination appears to overestimate the intensity of the $\alpha\beta$ peak relative to the $\gamma\delta\varepsilon$ peak. We were able to trace this discrepancy back to the partial charge used in the force fields. For example, when the above-mentioned scaling factor in the polarizable force fields is changed from 0.88 to 0.905 in the case of MdpA, the $\alpha\beta$ subpopulation is seen to decrease from 19.3% to 13.7%. However, in the present study we chose to use the 0.88 scaling factor because of its consistency with other structural and energetic properties of bulk methanol.

In order to further test the robustness of the MdpA force-field combination, we also used it in order to calculate the IR absorption spectra of the OH stretch in 10 different CD_3OH/CCl_4 mixtures in a concentration range between 1.17 and 80.08 mol % and compared the results to available experimental data.[16] The calculated spectra are shown in Figure 8 as well as the results of fitting them to two Lorentzian functions that correspond to the $\alpha\beta$ and $\gamma\delta\varepsilon$ peaks. The relative areas of the Lorentzian curve

dx.doi.org/10.1021/jp204245z |J. Phys. Chem. B 2011, 115, 9184–9194

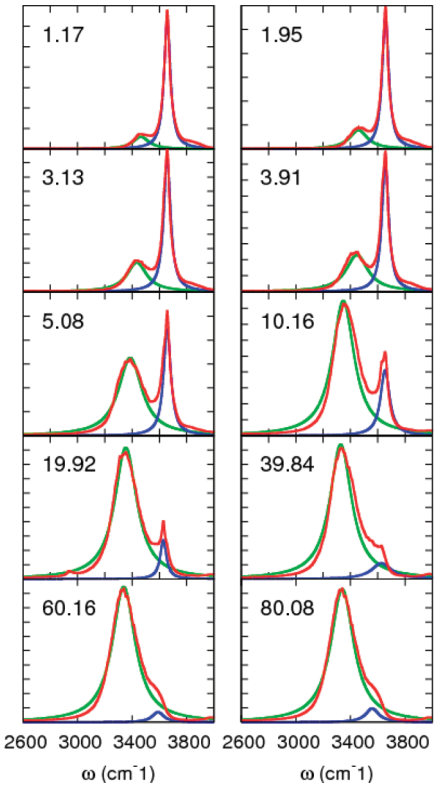

Figure 8. IR absorption spectra of the OH stretch in 10 different CD_3OH/CCl_4 mixtures in a concentration range between 1.17 and 80.08 mol %. The number in each panel corresponds to the concentration of CD_3OH in mol %.

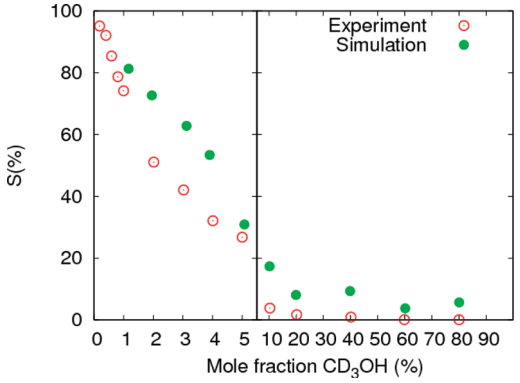

Figure 9. The proportion of areas of the $\alpha\beta$ band in the calculated IR absorption spectra of Figure 8. Experimental results are taken from ref 16.

for the $\alpha\beta$ peak are plotted in Figure 9 along with the corresponding experimental results reported in ref 16. As the concentration of methanol increases, the $\alpha\beta$ peak diminishes and the $\gamma\delta\varepsilon$ peak becomes broader and increasingly dominates the spectrum. Figure 9 shows that the calculated results systematically somewhat overestimate the experimental results, which is consistent with the observation of an overestimated $\alpha\beta$ peak discussed above. However, the overall trend is reproduced rather well, thereby providing further evidence for the robustness of our mixed quantum-classical procedure with the MdpA force-field combination.

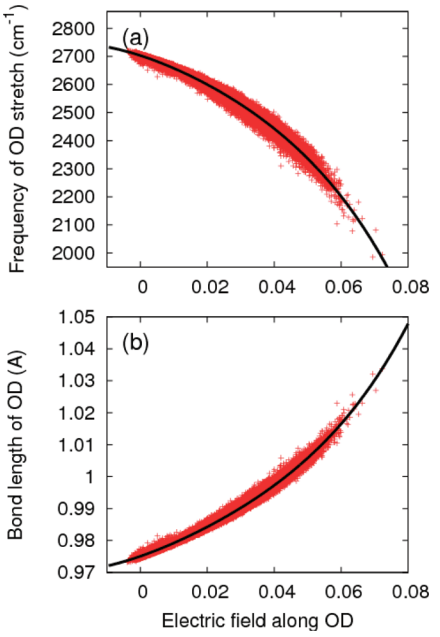

Figure 10. (a) A scatter plot of the OD stretch frequency as obtained from the mixed quantum-classical simulation vs the electric field along the OD bond in e/a_0^2 (red). The solid black line is the polynomial fit to the scatter plot. (b) A scatter plot of the expectation value of the OD bond length as obtained from the mixed quantum-classical simulation vs the electric field along the OD bond in e/a_0^2 (red). The solid black line is the polynomial fit to the scatter plot.

4. NONLINEAR MAPPING RELATIONS

The mixed quantum-classical procedure outlined in section 2A is rather expensive. One way of avoiding the on-the-fly diagonalization and thereby enhancing efficiency is by mapping the transition dipole moments and frequencies and Hellman−Feynman forces to collective order parameters. To this end, we observed that the fundamental transition frequency and OD bond length (defined as the expectation value of the bond length in the tagged molecule) are both strongly correlated with the electric field along the OD bond (see Figure 10). As a result, we were able to fit the relationship between the fundamental transition frequency and OD bond length and the electric field along the OD bond to the following fourth-order polynomials:

$$\omega(x) = 2703.029915692 - 3861.06974921979x - 73078.47175000155x^2 + 593316.6863306263x^3 - 10422964.358916607x^4 \quad (28)$$

$$r_{OD}(x) = 0.9750720279932595 + 0.36568724198663627x + 5.426784638525889x^2 - 52.00159545240706x^3 + 864.2659824749999x^4 \quad (29)$$

where the electric field x is given in units of e/a_0^2. Using these mapping relations, we were able to reproduce the absorption IR spectrum from a *classical* MD simulation based on the MdpA force-field combination, where we adjusted the OD bond length of the tagged MeOD at each time step based on eq 29, assigned the corresponding OD stretch frequency based on eq 28 (see Figure 11), and used the following approximation

dx.doi.org/10.1021/jp204245z |J. Phys. Chem. B 2011, 115, 9184–9194

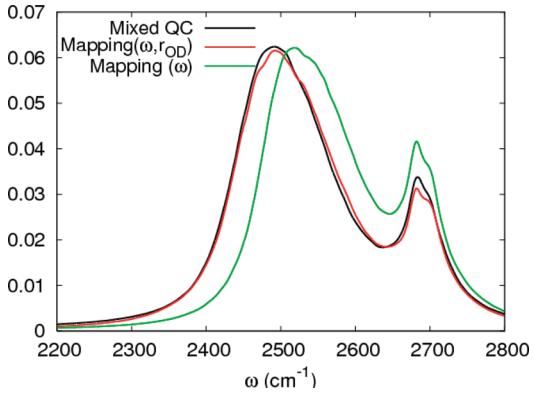

Figure 11. The IR absorption line shape as calculated by the mixed quantum-classical simulation (black) and by the classical simulation with the mapping relations between the electric field and the OD stretch frequency and the electric field and the OD bond length (red), for the case of 10 mol% MeOD/CCl_4. Also shown is the line shape calculated using only the mapping of the transition frequency (green).

in order to evaluate the Hellman−Feynman forces:

$$\langle\psi_n|\mathbf{F}_k(q,Q)|\psi_n\rangle \approx \mathbf{F}_k(\langle\psi_n|q|\psi_n\rangle, Q) \qquad (30)$$

We also found that only using the frequency mapping, eq 28, but keeping the OD bond length fixed at 0.96 Å, leads to a significantly less satisfactory reproduction of the spectrum (see Figure 11).

One notable feature is the fact that the relationship is nonlinear in contrast to other similar studies for the OH stretch in HOD/D_2O[50−52] and the amide I mode in *N*-methylacetamide[52−54] where the established relationships are linear. Another notable feature is that we employ the mapping relationship between electric fields and OD bond lengths in addition to the relationship between electric fields and OD stretch frequencies.

5. CONCLUDING REMARKS

While MD simulations are often employed nowadays for obtaining molecular level understanding of structural and dynamical trends in complex condensed phase systems, MD-based quantitative modeling of IR spectra remains a challenge. This is particularly true in the case of the high-frequency hydroxyl stretch in highly structured methanol/CCl_4 mixtures, where H-bonded oligomers form and break on the picosecond time scale. However, as the present study demonstrates, by combining mixed quantum-classical methodology with the appropriate choice of force fields, one can obtain a model which is at least consistent with the experimental absorption IR spectrum of the hydroxyl stretch for different isotopomers and on a wide range of compositions. In order to achieve this level of consistency without adjustable parameters, we found that one has to account for the anharmonic nature of the hydroxyl stretch and polarizable nature of the force fields, as well as the damping of the polarizability at short distances. This also implies that IR spectra can be used as highly sensitive and discriminative tests for the accuracy of force fields.

It should be noted that the mixed quantum-classical methodology employed here is limited in scope. More specifically, rather than treating all hydroxyl stretches quantum-mechanically, we only treat one hydroxyl quantum-mechanically, while the rest are treated classically. While this approach should be able to account for line broadening due to interactions with the other hydroxyls, it clearly cannot provide the fine energy level structure of the excitonic bands that a multihydroxyl quantum-mechanical treatment would afford. The ability of this approach to capture the experimental IR absorption spectrum rather accurately despite this seems to suggest that line broadening in this case is dominated by thermal classical solvent fluctuations, rather than by the intrinsic width of the excitonic band. It should also be noted that while limiting the quantum-mechanical treatment to a single hydroxyl significantly reduces the computational cost, the mixed-quantum-classical simulations are still rather expensive due to the need for diagonalizing the vibrational Hamiltonian on the fly. However, the existence of nonlinear mapping relations between the hydroxyl transition frequency and bond length and the electric field along the hydroxyl bond axis can be used to reduce the computational cost of the mixed quantum-classical treatment to that of a purely classical MD simulation.

Finally, it should be noted that while the absorption IR spectrum of the hydroxyl stretch is highly sensitive to H-bonding structure when the hydroxyl is in the ground vibrational state, it contains no information on H bonding in excited vibrational states and is also relatively insensitive to H-bonding dynamics (with the exception of partial quenching the $\alpha\beta$ peak due to rotational relaxation). However, one of the main advantages of the mixed quantum-classical methodology presented here is that it can be extended to excited states in a straightforward manner. In this context, it should be noted that H-bonded alcohol oligomers are believed to exhibit interesting photochemistry since the energy released upon the relaxation of the photoexcited hydroxyl stretch back to the ground state can result in breaking of H bonds in its vicinity.[17−21,28] Work on extending the mixed quantum-classical methodology presented herein to these processes which involve excited states and nonequilibrium H-bond dynamics and their spectral signature is currently underway and will be reported in future publications.

■ ACKNOWLEDGMENT

This project was supported by the National Science Foundation through grant CHE-0809506.

■ REFERENCES

(1) Jorgensen, W. L. *J. Am. Chem. Soc.* **1980**, *102*, 543–549.
(2) Palinkas, G.; Hawlicka, E.; Heinzinger, K. *J. Phys. Chem.* **1987**, *91*, 4334–4341.
(3) Haughney, M.; Ferrario, M.; McDonald, I. R. *J. Phys. Chem.* **1987**, *91*, 4934–4940.
(4) Matsumoto, M.; Gubbins, K. E. *J. Chem. Phys.* **1990**, *93*, 1981–1994.
(5) Staib, A. *J. Chem. Phys.* **1998**, *108*, 4554–4562.
(6) Meyer zum Büschenfelde, D.; Staib, A. *Chem. Phys.* **1998**, *236*, 253–261.
(7) Errera, J.; Mollet, P. *Nature* **1936**, *138*, 882.
(8) Liddel, U.; Becker, E. D. *Spectrochim. Acta Part A* **1957**, *10*, 70–84.
(9) Bellamy, L. J.; Pace, R. J. *Spectrochim. Acta* **1966**, *22*, 525–533.
(10) Bonner, O. D. *J. Chem. Thermodyn.* **1970**, *2*, 577–581.
(11) Veldhuizen, R.; de Leeuw, S. W. *J. Chem. Phys.* **1996**, *105*, 2828–2836.
(12) Dixon, J. R.; George, W. O.; Hossain, M. F.; Lewis, R.; Price, J. M. *J. Chem. Soc. Faraday Trans.* **1997**, *93*, 3611–3618.
(13) Graener, H.; Ye, T. Q.; Laubereau, A. *J. Chem. Phys.* **1989**, *91*, 1043–1046.

(14) Laenen, R.; Rauscher, C. *J. Chem. Phys.* **1997**, *106*, 8974–8980.
(15) Bertie, J. E.; Zhang, S. L. *J. Mol. Struct.* **1997**, *413*−*114*, 333–363.
(16) Kristiansson, O. *J. Mol. Struct.* **1999**, *477*, 105–111.
(17) Levinger, N. E.; Davis, P. H.; Fayer, M. D. *J. Chem. Phys.* **2001**, *115*, 9352–9360.
(18) Gaffney, K. J.; Davis, P. H.; Piletic, I. R.; Levinger, N. E.; Fayer, M. D. *J. Phys. Chem. A* **2002**, *106*, 12012–12023.
(19) Asbury, J. B.; Steinel, T.; Stromberg, C.; Gaffney, K. J.; Piletic, I. R.; Goun, A.; Fayer, M. D. *Phys. Rev. Lett.* **2003**, *91*, 23742.
(20) Asbury, J. B.; Steinel, T.; Stromberg, C.; Gaffney, K. J.; Piletic, I. R.; Fayer, M. D. *J. Chem. Phys.* **2003**, *119*, 12981–12997.
(21) Asbury, J. B.; Steinel, T.; Fayer, M. D. *J. Phys. Chem. B* **2004**, *108*, 6544–6554.
(22) Gulmen, T. S.; Sibert, E. L., III. *J. Phys. Chem. A* **2005**, *109*, 5777–5780.
(23) Gulmen, T. S.; Sibert, E. L., III. *J. Chem. Phys.* **2005**, *123*, 204508.
(24) Iwaki, L. K.; Dlott, D. D. *J. Phys. Chem. A* **2000**, *104*, 9101–9112.
(25) Iwaki, L. K.; Dlott, D. D. *Chem. Phys. Lett.* **2000**, *321*, 419–425.
(26) Wang, Z.; Pakoulev, A.; Dlott, D. D. *Science* **2002**, *296*, 2201–2203.
(27) Murdoch, K. M.; Ferris, T. D.; Wright, J. C.; Farrar, T. C. *J. Chem. Phys.* **2002**, 5717–5724.
(28) Graener, H.; Ye, T. Q.; Laubereau, A. *J. Chem. Phys.* **1989**, *90*, 3413–3416.
(29) Curtiss, L. A. *J. Chem. Phys.* **1977**, *67*, 1144–1149.
(30) Mo, O.; Yanez, M.; Elguero, J. *J. Mol. Struct. (THEOCHEM)* **1994**, *120*, 73–81.
(31) Ohno, K.; Shimoaka, T.; Akai, N.; Katsumoto, Y. *J. Phys. Chem. A* **2008**, *112*, 7342–7348.
(32) Staib, A.; Borgis, D. *Chem. Phys. Lett.* **1997**, *271*, 232–240.
(33) Jorgensen, W. L. *J. Phys. Chem.* **1986**, *90*, 1276–1284.
(34) McDonald, I. R.; Bounds, D. G.; Klein, M. L. *Mol. Phys.* **1982**, *45*, 521–542.
(35) Mukamel, S. *Principles of Nonlinear Optical Spectroscopy*; Oxford: New York, 1995.
(36) Schmidt, J. R.; Corcelli, S. A.; Skinner, J. L. *J. Chem. Phys.* **2005**, *123*, 044513.
(37) Hanna, G.; Geva, E. *J. Phys. Chem. B* **2008**, *112*, 12991–13004.
(38) Case, D.; Darden, T.; Cheatham, T.; III; Simmerling, C.; Wang, J.; Duke, R.; Luo, R.; Crowley, M.; Walker, R.; Zhang, W.; Merz, K.; Wang, B.; Hayik, S.; Roitberg, A.; Seabra, G.; Kolossváry, I.; Wong, K.; Paesani, F.; Vanicek, J.; Wu, X.; rozell, S.; Steinbrecher, T.; Gohlke, H.; Yang, L.; Tan, C.; Mongan, J.; Hornak, V.; Cui, G.; Mathews, D.; Seetin, M.; Sagui, C.; Babin, V.; .; Kollman, P. *AMBER 10*; University of California, San Francisco, 2008.
(39) Bauschlicher, C. W., Jr.; Langhoff, S. R.; Walch, S. P. *J. Chem. Phys.* **1992**, *96*, 450–454.
(40) Serrallach, A.; Meyer, R.; Günthard, H. H. *J. Mol. Spectrosc.* **1974**, *52*, 94–129.
(41) Caldwell, J. W.; Kollman, P. A. *J. Phys. Chem.* **1995**, *99*, 6208–6219.
(42) Duffy, E. M.; Severance, D. L.; Jorgensen, W. L. *J. Am. Chem. Soc.* **1992**, *114*, 7535–7542.
(43) Applequist, J.; Carl, J. R.; Fung, K. K. *J. Am. Chem. Soc.* **1972**, *94*, 2952.
(44) Alfredsson, M.; Brodholt, J. P.; Hermanson, K.; Vallauri, R. *Mol. Phys.* **1998**, *94*, 873–876.
(45) Bernardo, D. N.; Ding, Y.; Krogh-Jespersen, K.; Levy, R. M. *J. Phys. Chem.* **1994**, *98*, 4180–4187.
(46) Masia, M.; Probst, M.; Rey, R. *J. Chem. Phys.* **2005**, *123*, 164505.
(47) Thole, B. T. *Chem. Phys.* **1981**, *59*, 341–350.
(48) Cieplak, P.; Dupradeau, F.-Y.; Duan, Y.; Wang, J. *J. Phys.: Condens. Matter* **2009**, *21*, 333102.
(49) Berendsen, H. J. C.; Postma, J. P. M.; van Gunsteren, W. F.; DiNola, A.; Haak, J. R. *J. Chem. Phys.* **1984**, *81*, 3684–3690.
(50) Corcelli, S. A.; Skinner, J. L. *J. Phys. Chem. A* **2005**, *109*, 6154–6165.
(51) Corcelli, S. A.; Lawrence, C. P.; Skinner, J. L. *J. Chem. Phys.* **2004**, *120*, 8107–8117.
(52) Schmidt, J. R.; Corcelli, S. A.; Skinner, J. L. *J. Chem. Phys.* **2004**, *121*, 8887–8896.
(53) Ham, S.; Kim, J.-H.; Lee, H.; Cho, M. *J. Chem. Phys.* **2003**, *118*, 3491–3498.
(54) Bour, P.; Keiderling, T. A. *J. Chem. Phys.* **2003**, *119*, 11253–11262.